FISEVIER

Contents lists available at ScienceDirect

# **Materials Today Communications**

journal homepage: www.elsevier.com/locate/mtcomm



# Tin asymmetric membranes for high capacity sodium ion battery anodes

Mengya Li<sup>b,1</sup>, Christopher Anderson<sup>a,1</sup>, Parker Beaupre<sup>a</sup>, Congrui Jin<sup>c</sup>, Jianlin Li<sup>b,\*</sup>, Ji Wu<sup>a,\*</sup>



- <sup>a</sup> Department of Chemistry and Biochemistry, Georgia Southern University, 250 Forest Drive, Statesboro, GA, 30460, USA
- <sup>b</sup> Energy & Transportation Science Division, Oak Ridge National Laboratory, Oak Ridge, TN, 37831, USA
- <sup>c</sup> Department of Mechanical Engineering, Binghamton University, 4400 Vestal Parkway East, Binghamton, NY, 13902, USA

#### ARTICLE INFO

Keywords:
Tin
Asymmetric membrane
Anode
Sodium ion Battery
High capacity

#### ABSTRACT

Sodium-ion batteries have attracted tremendous research attention as promising candidates for next generation energy storage systems due to low-cost and high abundancy. However, comparing to current Li-ion battery technology, limitations on the anode side seriously hinder the cell performance since sodium does not easily intercalate into graphite materials. Here, tin nanoparticles embedded in various asymmetric membrane structures were developed to leverage the high capacity of tin (847 mA h g $^{-1}$  based on Na<sub>15</sub>Sn<sub>4</sub>) and accommodate the significant volume expansion for long cycle life. It was demonstrated 762 mA h g $^{-1}$  reversible capacity at 50 mA g $^{-1}$  and stable cycling performance over 100 cycles with 92.1% capacity retention at 100 mA g $^{-1}$  can be achieved for the tin asymmetric membrane electrode synthesized using polysulfone and tin tert-butoxide precursor.

# 1. Introduction

In the last decades we have witnessed a worldwide rapid growth in the energy density of rechargeable batteries [1]. The advancement is mainly driven by increasing demands for portable electronics, electric vehicles and energy storage systems for intermittent power sources [2]. Although powerful, reliable and highly rechargeable lithium ion batteries (LIBs) are currently dominating the market, serious concerns have been raised over its sustainability owing to the low abundance of lithium and entailing high cost [3,4]. Therefore scientists are making tremendous efforts in search of alternative technologies with lower cost, higher sustainability and uncompromised electrochemical performance as compared to LIBs. Among those, sodium ion battery (SIB) stands out as a promising candidate for large-scale next-generation electrochemical energy storage, mainly due to the rich abundance of sodium and a potential cost reduction of 12.5% comparing to LIBs [5-8]. Although exciting developments have been achieved with SIB cathode materials, significant challenges remain in identifying appropriate SIB anode materials [9,10]. In this regard, group IV element, tin can play an important role, owing to its outstanding theoretical capacity of 847 mA h g<sup>-1</sup> based on Na<sub>15</sub>Sn<sub>4</sub> [6]. However, Sn anode does suffer from large volume changes (523%) during the sodiation and desodiation and thus experience troublesome cycling stability issues as confirmed by both theoretical and experimental investigations [11–13].

Quite a few creative strategies have been proposed to relieve the large volume change problem, most of which focus on different kinds of nanostructuring, such as Sn nanofibers synthesized using template or template-free methods [14,15], Sn nanoparticles embedded in natural wood fibers [16], 3-D spherical multideck-cage particles prepared using electrostatic spray deposition technology, [17] 3-D porous graphene network anchored with Sn nanoparticles [18], Sn embedded in porous carbon or carbon nanotubes [19–22], SnO<sub>2</sub>-graphene composite. [23,24] However, research on a large scale synthesis of Sn-based SIB anodes with high performance for commercial applications is still seriously lacking [25,26].

Traditional reverse osmosis asymmetric membranes can be fabricated on a large scale via a roll-to-roll processing technology through a simple phase inversion or interfacial grafting method [27]. This well-established technology has recently been adapted by our research group to enhance the cyclability of high capacity alloying anodes for LIBs [28]. In this report, the scalable and efficient approach was employed to synthesize four types of Sn asymmetric membranes using different kinds of polymers and tin precursors for high capacity SIB anodes. Polysulfone and polyacrylonitrile were selected because they have been widely adopted to fabricate reverse osmosis membranes for water desalination, whose phase inversion dynamics and morphologies have been extensively studied [29]. Reverse osmosis membranes fabricated using polysulfone are usually characterized by fast phase inversion

<sup>\*</sup> Corresponding authors.

E-mail addresses: lij4@ornl.gov (J. Li), jwu@georgiasouthern.edu (J. Wu).

<sup>&</sup>lt;sup>1</sup> These authors contributed equally to this work.

dynamics and thus possesses high porosity, whereas membranes made using polyacrylonitrile have slow phase inversion dynamics and entailing low porosity [30,31]. However, the mechanical strength of reverse osmosis membranes fabricated using polyacrylonitrile is stronger than that of polysulfone [32,33]. Additionally, two tin precursors with different chemical reactivity (tin (IV) 2-ethylhexanoate diisopropoxide and tin (IV) tert-butoxide) were chosen to study their effect on the membrane porosity and concentration of tin in the membrane. The membranes were characterized by scanning electron microscope (SEM), energy dispersive X-ray spectroscopy (EDS), Raman spectroscopy, powder X-ray diffractometer (PXRD), thermogravimetric analyzer (TGA), X-ray photoelectron spectroscopy (XPS), and various electrochemical analyses as well. It was demonstrated that tin asymmetric membranes made from tin tert-butoxide and polysulfone delivered the highest initial reversible capacity of 762 mA h g<sup>-1</sup> while the ones using tin (IV) 2-ethylhexanoate diisopropoxide and polyacrylonitrile exhibited the highest capacity retention after 100 cycles, 79.1%, 92.1% and 83.8% at 50, 100 and 200 mA g<sup>-1</sup>, respectively. The highly porous structure of these asymmetric membranes not only enabled efficient Na diffusion paths, but also accommodated the large volume expansion of Sn-based SIB anodes. In addition, the thin oxide layer at the surface of tin nanoparticles embedded in the asymmetric membranes acted as a protective layer for relieving the volume expansion during the alloying reaction with Na+. Our study clearly demonstrated a novel and scalable approach to engineer the electrode architecture of tinanode to maximize the reversible capacity and stabilize the cycling performance, which can be a promising avenue for building future SIBs with a high energy density.

#### 2. Material and methods

#### 2.1. Fabrication of thin film asymmetric membranes

PS tert-butoxide and PAN tert-butoxide tin membranes: A uniform slurry was obtained by ball-milling a mixture of 1.0 g polysulfone (PS,  $M_n \approx 60,000$ , pellets, Acros) or 0.50 g polyacrylonitrile (PAN,  $M_n \approx$ 150,000, powders, Pfaltz & Bauer), 0.25 g carbon black (CB, SUPER C45 with a surface area of 45 m<sup>2</sup> g<sup>-1</sup>, Imerys Graphite & Carbon), 2.0 g Sn (IV) tert-butoxide and 10 mL of N-methyl-2-pyrrolidone (NMP, Sigma Aldrich, > 99.5%) were ball-milled at 50 rpm for 3 h (Across International, PQ-N04 Planetary Ball Mill). Then, the slurry was coated onto a piece of 4-inch diameter silicon wafer using a doctor blade with a 200 µm gap. The wafer was then immersed into 1 L de-ionized water ( > 17 M $\Omega$ .cm) for ~30 min to initiate the phase inversion, resulting in the formation of porous asymmetric membranes. As-prepared membranes were carbonized at 500 °C for 2 h using a Lindberg/Blue M™ 1100 °C tube furnace with a ramp rate of ~60 °C min<sup>-1</sup> to generate conductive tin asymmetric membranes. Samples were protected by 200 sccm helium gas (99.9999%, Airgas He UHP300) during the carbonization. PAN 2-ethylhexanoate diisopropoxide tin membrane: The procedure was the same as the one for PAN tert-butoxide tin membrane except that tin (IV) tert-butoxide was replaced by tin (IV) 2-ethylhexanoate diisopropoxide (98%, Alfa Aesar). PS/CB and PAN/CB reference membranes: The reference membranes were fabricated following the same aforementioned procedures but no tin precursor.

### 2.2. Fabrication of fibrous membrane

PAN 2-ethylhexanoate diisopropoxide tin fibrous membrane: The slurry was identical to the one used for PAN 2-ethylhexanoate diisopropoxide tin thin film membrane as described above. To obtain fibrous asymmetric membrane, the slurry was filled into a plastic syringe whose barrel was fortified by a metal cylinder, and then extruded through a 33 G needle using a homebuilt device shown in Fig. 1. One-ton manual arbor press was utilized to extrude the viscous slurry into deionized water to produce the fibrous asymmetric membrane. The fibers were

carbonized at  $500\,^{\circ}$ C for 2 h under the protection of helium gas of  $200\,\text{sccm}$  to make them electrically conductive Table 1.

#### 2.3. Characterization of asymmetric membranes

Field Emission Scanning Electron Microscope (FESEM, JEOL JSM-7600 F) attached with an Energy Dispersive X-ray analyzer and a transmission electron detector (TED) was used for morphological and compositional characterization. The concentration of Sn in asymmetric membranes was quantified using a thermogravimetric analyzer (TA Instruments Q50 TGA) that was operated using high purity compressed air gas (Ultra Zero, Airgas) at a flow rate of 20 mL min<sup>-1</sup>. The oven temperature was ramped at a rate of 10 °C min<sup>-1</sup> to 120 °C, held for 10 min, and then increased to 700 °C, held for 30 min. A Thermo Scientific DXR SmartRaman Spectrometer was operated using a 532 nm laser of 1 mW, an objective lens of  $\times$  10, an aperture size of 25  $\mu$ m and a total exposure time of 300 s in the range of 100 to 3500 cm<sup>-1</sup>. Powder X-ray diffraction patterns (PANanalytical Empyrean) were collected using a Cu  $K_{\alpha}$  radiation ( $\lambda = 1.540598 \text{ Å}$ ) from 10 to 90° (two theta) with a step rate of  $0.1^{\circ}$  s<sup>-1</sup> for 32 times to enhance signal to noise ratio. The acceleration voltage and current were 40 kV and 40 mA, respectively. Samples were also analyzed using an X-ray photoelectron spectroscopy (XPS, Scienta Omicron ESCA-2SR) with an operating pressure of  $\sim 1 \times 10^{-9}$  Torr and monochromatic Al  $K_{\alpha}$  X-rays (1486.6 eV). Photoelectrons were collected from a 5 mm diameter analysis area and at a 0° emission angle with source to analyzer angle of 54.7 degrees. A hemispherical analyzer was used to determine photoelectron kinetic energy. A pass energy of 200 V was employed for wide/survey scans, and 50 V for high resolution scans. The specific surface areas of asymmetric membranes were measured using a Micromeritics ASAP 2020 Surface Area and Porosimetry Analyzer at Binghamton University. All samples were degassed at 50 µTorr and 300 °C for 30 min before the measurements.

# 2.4. Electrode preparation and electrochemical testing of anodes

An adhesive slurry was prepared by mixing 0.8 g carbon black (Super C60) and 0.5 g polyvinylidene fluoride (PVDF, SOLEF 9130) with 15 mL NMP in SPEX mill for 10 min. Sodium anodes were fabricated by gluing the membrane to a thin layer of the adhesive slurry which was casted onto aluminum disks (14 mm in diameter and 15  $\mu m$  thick). The assembled anodes were dried at 100 °C in a dry room overnight before transferring to the glovebox. The average active material loading on each disk is around 65 wt%. Electrochemical tests were performed on coin cells with Na metal as the working electrode, 1 M NaClO<sub>4</sub> (> 98%, Sigma-Aldrich) in poly (propylene carbonate) (PPC) with 5 wt% fluoroethylene carbonate (FEC, BASF) as electrolyte, and glass fiber (Whatman GF/F) as separator. Galvanostatic tests were performed between 0.01–3 V against Na/Na $^+$  at various current densities (50, 100, 200 mA  $g_{\rm active}^{-1}$ ).

#### 3. Results and discussion

#### 3.1. Fabrication of tin asymmetric membranes

Thin film tin asymmetric membranes were prepared using a simple phase inversion method like the one described in our previous work (Fig. 1a) [28]. To produce fibrous tin asymmetric membrane, a homebuilt extrusion system was manufactured to extrude the viscous slurry under the requisite high pressure through 33 G needle (Fig. 1b and c). It is notable that both thin film and fibrous asymmetric membranes can be fabricated continuously on a large scale using a roll-to-roll processing like the fabrication of reverse osmosis membrane for water desalination and purification [34]. The addition of carbon black is necessary to maintain the asymmetric porous structure during the following high temperature carbonization and increase the electrical conductivity of

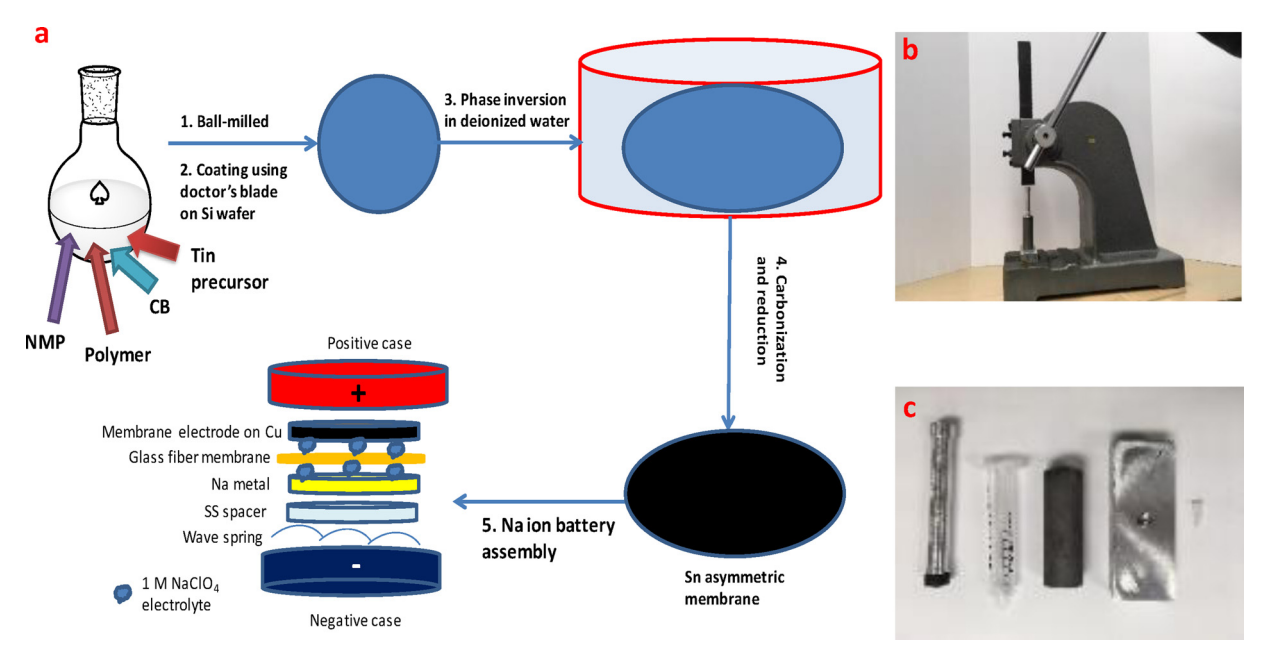


Fig. 1. a) Schematic for the fabrication of thin film Sn asymmetric membranes b) and c) are photo images of the setup and components used to prepare fibrous Sn asymmetric membranes, respectively.

 Table 1

 Asymmetric membranes prepared for this study.

Sample Name		Sample Label	Polymer	Tin precursor	Thickness (µm)	Filler
PS butoxide tin membrane		PSBT	PS	Tin(IV) tert-butoxide	200	СВ
PAN butoxide tin membrane		PANBT	PAN	Tin(IV) tert-butoxide	200	CB
PAN 2-ethylhexanoate diisopropoxide tin membrane		PANET	PAN	Tin(IV) 2-ethylhexanoate diisopropoxide	200	СВ
PAN 2-ethylhexanoate diisopropoxide tin fibrous membrane		PANET Fiber	PAN	Tin(IV) 2-ethylhexanoate diisopropoxide	200	СВ
PAN/CB membrane PS/CB membrane		PAN/CB PS/CB	PAN PS	None None	200 200	CB CB
	PS PS					
PAN	Tin(IV) tert-butoxide Tin(IV) 2-ethylhexanoate diisopropo	xide				

membranes for an improved rate performance. The asymmetric membrane prepared using polysulfone (PS) is much more porous than the one obtained from PAN because the exchange of NMP and water (demixing) is much faster in PS solution as reported in literature [29]. However, the mechanical strength of carbonized PAN tin membrane is much stronger than that of carbonized PS tin membrane since PAN is an excellent precursor for the fabrication of graphitic carbon fibers with

outstanding mechanical strength [35,36]. Two kinds of organometallic tin precursors (tin(IV) tert-butoxide and tin (IV) 2-ethylhexanoate dissopropoxide) with different chemical reactivity were used to prepare tin asymmetric membranes for comparison. Tin (IV) tert-butoxide is highly moisture sensitive compared to tin (IV) 2-ethylhexanoate diisopropoxide, thereby leading to rapid formation of sol-gel during the phase inversion in deionized water and resulting in higher porosity.

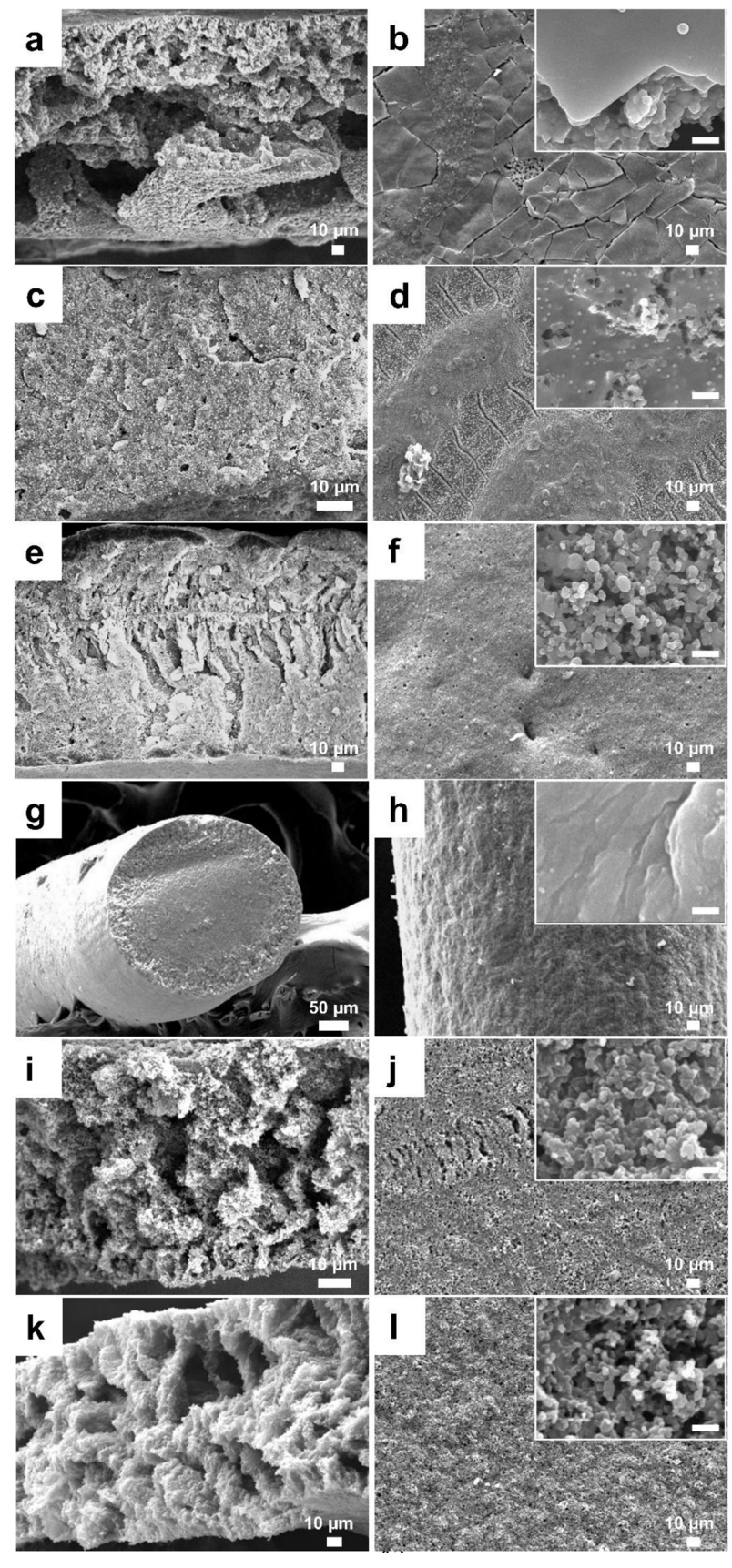


Fig. 2. Scanning electron microscope images of a)-b) PS tert-butoxide (PSBT); c)-d) PAN tert-butoxide (PANBT); e)-f) PAN 2-ethylhexanoate diisopropoxide tin membranes (PANET); g)-h) PAN 2-ethylhexanoate diisopropoxide tin fibrous membrane (PANET fiber); i)-j) PS/CB and k)-l) PAN/CB reference membranes. Note: Left to right in the same row are cross-sectional and top-view images. Insets are high-resolution top-view images (scale bars are 500 nm).

#### 3.2. Characterization of tin asymmetric membranes

As revealed by SEM imaging (Fig. 2), the membrane prepared using PS is more porous than the one made from PAN, which is consistent with literature report and our previous studies [28,37,38]. The PSBT membrane also exhibited some cracks on the surface where Sn nanoparticles could be leached out to the electrolyte during the repeated sodiation/de-sodiation (Fig. 2a). The type of tin precursor also has certain effect on the membrane porosity. The use of tin (IV) ethylhexanoate diisopropoxide benefits the formation of slightly more porous structure as compared to tin (IV) tert-butoxide (Fig. 2a and c). Also, the PANET membrane showed a more integrated surface (Fig. 2c) which may provide a better protection of Sn nanoparticles. The fibrous tin membrane was characterized as the lowest porosity compared to thin film tin asymmetric membranes due to the formation of dense nanoporous shell that can hinder the exchange of NMP and water and thereby reduce the overall porosity (Fig. 2f and h). Two reference membranes, PS/CB and PAN/CB were also fabricated for comparison. It can be clearly seen that the reference membranes were much more porous than the tin asymmetric membranes because the pores of tin asymmetric membranes were partially filled by Sn-SnO2 particles (Fig. 2i-l).

Sn concentration in these asymmetric membranes was quantified using a thermogravimetric analyzer that utilizes compressed air as the purging gas. As shown in Table 2 and Fig. 3, the concentrations of Sn in PSBT and PANBT membranes were comparable to each other (34.8 vs. 39.8 wt.%); whereas PANET membrane contains only 21.7 wt.% tin. The low chemical reactivity of tin (IV) ethylhexanoate diisopropoxide compared to tin (IV) tert-butoxide may slow down the formation of viscous sol-gel and cause extra loss of precursor during the phase inversion stage. However, the content of tin in PANET fibrous membrane was much higher than that in PANET thin film membrane (43.2 wt.% vs. 21.7 wt%). It is believed that the formation of dense nanoporous shell can prohibit the loss of tin precursor, and thus increase tin concentration. The concentration of tin in reference membranes was basically zero because no tin precursor was utilized in those membranes.

Raman spectra of asymmetric membranes are shown in Fig. 4a. Peaks centered at ~1600 and 1350 cm<sup>-1</sup> can be attributed to graphitic G and D peaks, respectively [39,40]. The G/D ratio of the membranes fabricated using PS is significantly higher than that of PAN membranes, indicating that PS membranes contain more graphitic-like materials. Among these membranes, only PSBT membrane contains a large amount of SnO2 that can be detected by Raman scattering spectroscopy (160 and 303 cm<sup>-1</sup>) [41]. Powder X-ray diffraction data confirm the presence of amorphous carbon, crystalline β-tin, trace amount of oxidized tin as well in all tin asymmetric membranes that are fabricated using PAN (Fig. 4b) [42]. The broad patterns also indicate the presence of nanoscale tin. In contrast, PSBT membrane contains a large amount of tin dioxide besides elemental tin, which is consistent with the above Raman data. Noteworthy, oxidized tin may reduce the overall electrode volume expansion and lead to the formation of Na<sub>2</sub>O, both of which can help stabilize electrode cyclability as reported in literature [43]. PXRD patterns also confirm that PAN/CB and PS/CB reference membranes are composed of carbon only. The average particle size of tin in PSBT asymmetric membrane was calculated to be ~28 nm using (200) diffraction peak at 30.6° (Fig. 4b) and Scherrer equation shown below:

**Table 2**Thermogravimetric analyses of various asymmetric membranes prepared using different polymer, tin precursor and geometry.

Sample Label	PSBT	PANBT	PANET	PANET Fiber	PAN/CB	PS/CB
Content of Sn (wt. %)	34.8	39.8	21.7	43.2	0	0

$$D = \frac{K\lambda}{\beta cos\theta}$$

where D represents the mean size of Sn nanocrystals, K is the dimensionless shape factor (0.9),  $\lambda$  is the X-ray wavelength,  $\beta$  is the line width at half the maximum intensity from (200) diffraction and  $\theta$  is the Bragg angle of (200) plane [44,45]. The typical size of Sn nanoparticles was also estimated by TEM imaging to be around 40-50 nm as shown in **Figure S6**, which size is close to the average one calculated using PXRD data and Scherrer equation.

The oxidation states of Sn on the top surface of asymmetric membranes were identified using Sn (3d) XPS spectra (Fig. 4c). The binding energy values of Sn  $^3d_{5/2}$  and  $^3d_{3/2}$  were found to be 486.7 and 495.2 eV, respectively, being consistent with literature reports [46,47]. XPS data point out that the surface of elemental tin in the asymmetric membranes are fully oxidized.

BET surface area analyses (Table 3) indicate both PSBT and PS/CB membranes have extremely high specific surface areas ( $>300~{\rm m}^2~{\rm g}^{-1}$ ), being consistent with their highly porous structure as shown in Fig. 2. In contrast, the specific surface area of PAN/CB is more than one order of magnitude lower due to its low porosity as confirmed by SEM imaging (Fig. 2). Tin asymmetric membranes fabricated using PAN (PANBT, PANET, PANET Fiber) have quite similar surface areas that are slightly higher than that of PAN/CB control membrane because of the existence of Sn nanoparticles.

#### 3.3. Electrochemical properties of tin asymmetric membranes as SIB anode

Galvanostatic charge/discharge tests were performed for PSBT, PANBT, PANET, PANET fiber, PAN/CB, and PS/CB in SIB half cells. As a reference, the electrochemical performance of pristine PAN/CN and PS/ CB with no Sn content was also evaluated (Fig. 5a, b and Figure S1). The large 1st cycle irreversibility that results from SEI formation at the carbon-electrolyte interface only lead to 230 and 145 mAh g<sup>-1</sup> reversible capacity for PAN/CB and PS/CB, respectively. All the specific capacity values for tin-containing anodes were normalized to the mass of tin only and after subtracting the contribution from the carbon sources. The 1st cycle discharge capacity for PSBT, PANBT, PANET, and PANET fiber was 1009, 537, 980, 653 mA h  $g^{-1}$ , respectively (see Fig. 5). Due to the formation of SEI for both carbon and tin in the anode and the associated capacity loss, the 1st cycle charge capacity for PSBT, PANBT, PANET, and PANET fiber was 713, 372, 501, and 271 mAh g<sup>-1</sup>, with corresponded 1st cycle Coulombic efficiency (CE) of 71, 69, 51, and 41%, respectively. PSBT demonstrated the highest 1st-cycle CE and reversible capacity (see Fig. 5c), which could be a synergistic effect of the porous structure, thin surface oxide coating and the existence of more graphitic materials. The structural confinement and surface protection can accommodate the volume expansion of Sn during alloying with sodium. Compared to PSBT, PANBT also exhibited high and comparable initial CE in the 1st cycle (Fig. 5d). As PSBT and PANBT have the same Tin precursor, the comparable CE could indicate similar properties of Sn in both samples. The lower specific capacity in PANBT indicated less utilization of Sn. In addition, the cycling performance of PANBT was much worse than the PSBT remaining less than 100 mA h g<sup>-1</sup> discharge capacity at the 3rd cycle. This is ascribed to the much denser membrane structure (Fig. 2) resulted from the PAN membrane, which couldn't accommodate the significant volume expansion of Sn. The denser structure and lower surface area of PANBT showed higher CE in the first cycle than PSBT (65.0% vs 48.2%) if the whole electrode capacity was counted. Thus, utilizing PS as the polymer created more porous membrane structure which increased utilization of Sn and improved cyclability. When switching the Tin precursor from Tin (V) tertbutoxide to 2-rthylhexanoate diisopropoxide, PANET (Fig. 5e) delivered higher initial discharge capacity, more stable in the first three cycles but lower 1st cycle CE. This indicated that the Sn generated from the 2-rthylhexanoate diisopropoxide was more accessible. The lower

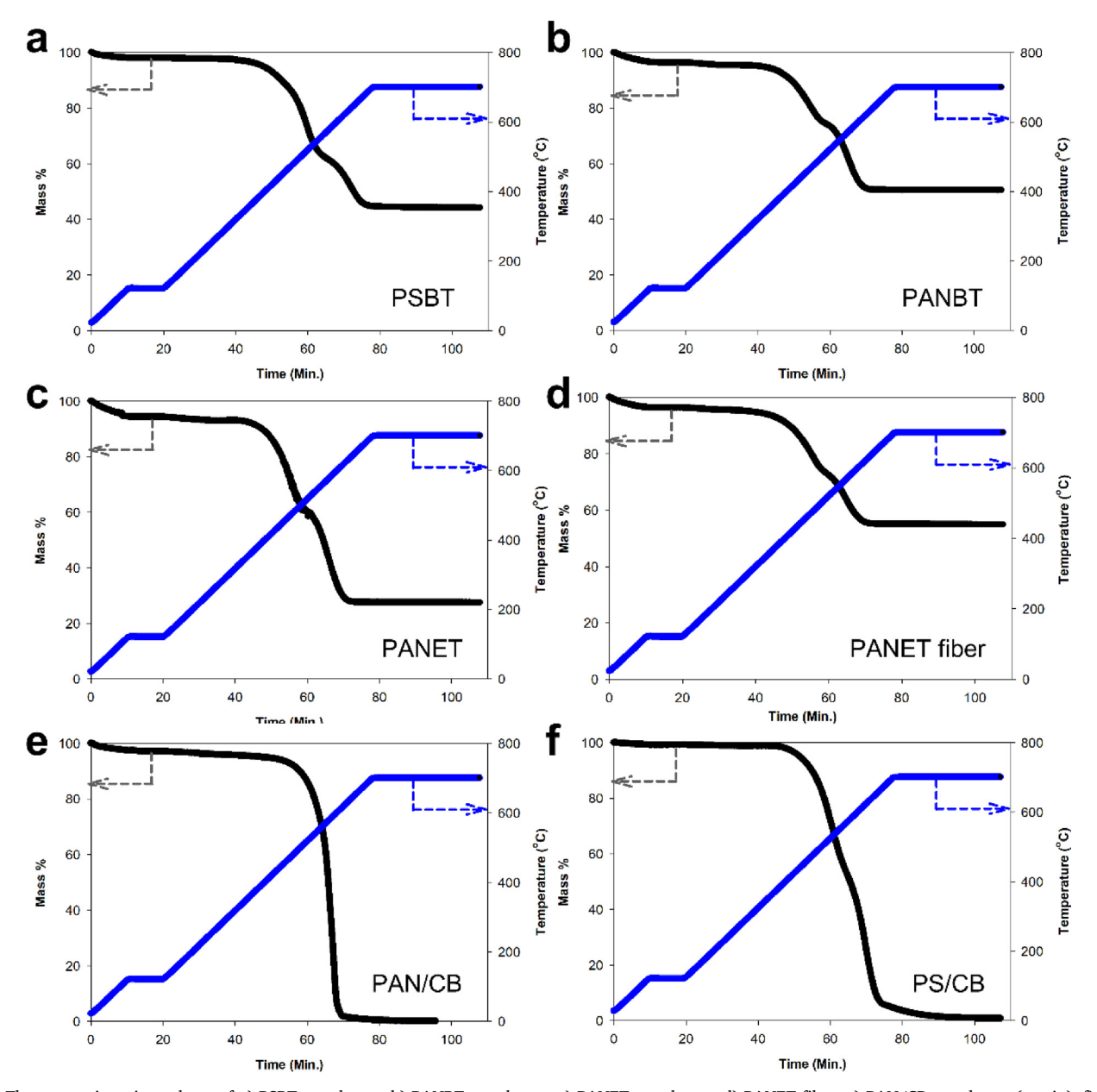


Fig. 3. Thermogravimetric analyses of a) PSBT membrane; b) PANBT membrane; c) PANET membrane; d) PANET fiber; e) PAN/CB membrane (no tin); f) PS/CB membrane (no tin).

capacity compared to the PSBT was ascribed to the different membrane structure, i.e. less porous and surface area. With the same PANET but fibrous morphology, the cell exhibits poor initial discharge capacity and fast capacity decay within the first three cycles (Fig. 5f). The poor electrochemical performance of PANET fiber comparing to PANET could be attributed to the inefficient structure confinement of fibers perpendicularly, which may further lead to expansion of the composite electrode and active material delamination from the current collector. The capacities normalized to the total mass of electrodes are shown in Figure S3 for comparison.

Based on the galvanostatic charge/discharge results, we further performed cycling performance test at various rates (50, 100, 200 mA  $g_{Sn}^{-1}$ ) on the two high capacity anodes-PSBT and PANET. The cycling data shown in Fig. 6a indicates stable cycling over 100 cycles for PSBT. The capacity retention for PSBT was 56.8, 70.3, and 51.1% at 50, 100, and 200 mA  $g_{Sn}^{-1}$ , respectively. It is worth to notice that at 100 mA  $g_{Sn}^{-1}$ , the PSBT cell maintained 482 mA h  $g_{Sn}^{-1}$  after 100 cycles. For PANET (see Figure S2), the capacity retention at 50, 100, and 200 mA/

 $g_{Sn}$  was 79.1, 92.1, and 83.8%, respectively. Notably, at 100 mA  $g_{Sn}^{-1}$ , the PANET cell maintained 462 mA h g<sup>-1</sup> after 100 cycles. The PSBT composite membrane can accommodate the volume expansion of tin nanoparticles by protection of both surface oxidation layer and flexible interconnected asymmetric membrane (see schematic illustration in Fig. 6b). The lower capacity retention at 50 mA g<sup>-1</sup> was due to higher utilization of Sn (higher capacity) which could result in particle pulverization and associated loose contact and electrically deactivation. As the PSBT showed higher initial capacity than PANET, the capacity fade was also more pronounced. When cycled at high current (200 mA g<sub>Sn</sub><sup>-1</sup>), the capacity was lower which reduced the volume expansion and was beneficial to cyclability. However, the fast sodiation and desodiation may not leave enough time for the particles to relax and accommodate the strain, which could lead to more particle fracture and resulted in low capacity retention. When cycled at intermediate current  $(200\,\text{mA g}_{\text{Sn}}^{-1})$ , a combination of relatively lower utilization of Sn compared to the low current and longer relaxation time for the particles to accommodate strain compared to high current produced the best

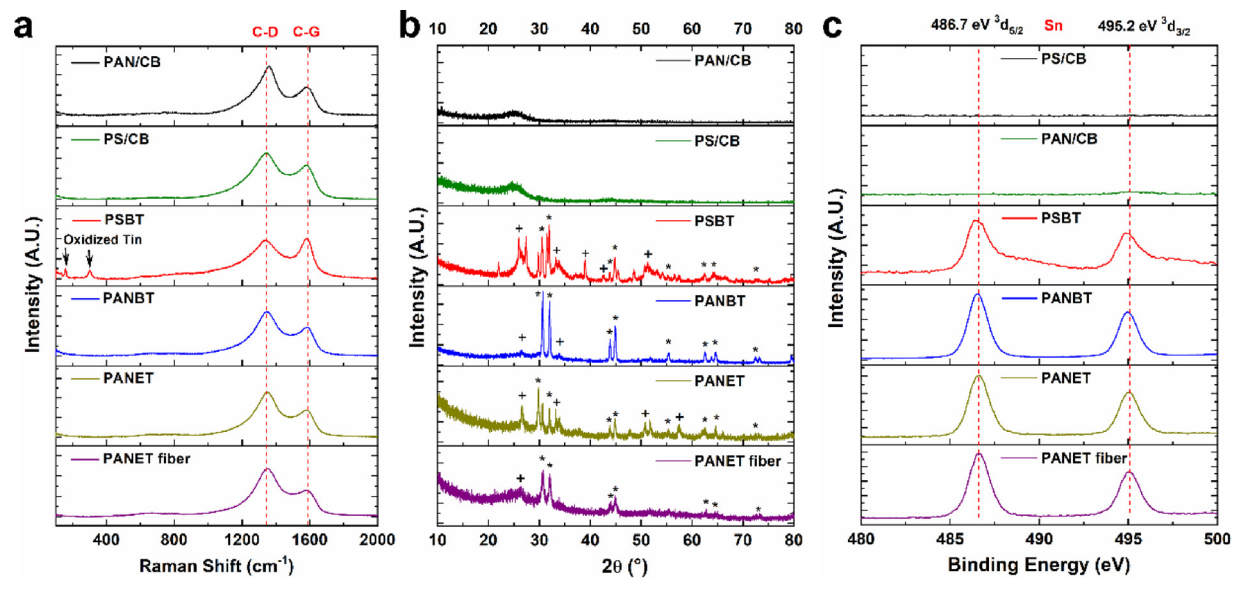


Fig. 4. a) Raman spectra, b) powder X-ray diffraction patterns and c) Sn (3d) X-ray photoelectron spectra of asymmetric membranes prepared using different polymer, tin precursor and geometry. \* Patterns from beta tin (JCPDS No. 00-004-0673); + patterns from tetragonal SnO<sub>2</sub> (JCPDS No. 41-1445).

**Table 3**BET (Brunauer, Emmett and Teller) specific surface areas of asymmetric membranes.

	PSBT	PANBT	PANET	PANET Fiber	PAN/CB	PS/CB
Specific Surface	312.23		46.16	67.53	27.19	357.01
Area (m <sup>2</sup> g <sup>-1</sup> )	± 0.82		± 0.16	± 0.29	± 0.06	± 0.82

capacity retention and capacity. PANET showed lower capacity compared to PSBT when cycled at the same current. The lower utilization of Sn in PANET enabled higher capacity retention. For better reference, the galvanostatic charge/discharge profiles were shown as **Figure S3**.

Besides charge/discharge profiles, the dQ/dV profiles of the anodes were presented in Figure S4. For pure carbon anodes (Figure S4a-b), the discharge peaks between 0.5 to 1 V in the first cycle indicated SEI formation on the carbon/electrolyte interface, which disappeared in the following cycle. For tin-containing anodes (Figure S4c-f), discharge peaks below 0.5 V in the first cycle was due to the formation of SEI layer on the tin/electrolyte interface, which were absent in the following cycle. The first cycle irreversible capacities are associated with the SEI formation at the interface. Among all the tin-containing anodes (Figure S4c-f), it is worth to note that the capacity reversibility is relatively high for PSBT and PANET anodes, as dictated by the almost overlapped dQ/dV profiles for the 2<sup>nd</sup> cycle compared to the 1<sup>st</sup> cycle despite the SEI formation. The morphologies of the anode materials after cycling was characterized by SEM, as shown in Figure S5. For our PSBT electrode with the best performance, several microcracks were developed after long-term cycling. However, the integrity of the electrode was maintained (Figure S5a), as Sn/SnO2 nanoparticles still being covered by the polymer sheets (Figure S5b). In comparison, PANET electrode has also maintained overall electrode integrity (Figure S5c). But Sn/ SnO<sub>2</sub> nanoparticles were largely exposed on the surface as microcracks developed (Figure S5d). Moreover, for PANET fiber electrode, it is noticeable that macrocracks were developed after cycling (Figure S5e) along with the exposure of Sn particles, which potentially caused more SEI formation that led to irreversibility and poor cycling. Overall, we developed this novel tin composite anode architecture that could future be scaled-up for fabricating high-performance sodium-ion batteries. While the electrochemical performance needs further improvement, the performance of PSBT and PANET was comparable to the results reported in literature summarized in Table S1 [48-51].

#### 4. Conclusions

An asymmetric membrane structure was developed for tin anode to leverage the high capacity of tin and accommodate the significant volume expansion for long cycle life. The effect of polymer and tin precursors on tin anode performance was investigated. It was demonstrated that the asymmetric membranes using polysulfone were more porous than those with polyacrylonitrile. The more porous structure could better accommodate the volume expansion of tin anode and enabled superior cyclability albeit lower 1 st cycle coulomb efficiency. Utilization of tin was higher with 2-rthylhexanoate diisopropoxide as the precursor. High capacity (762 mA h g $^{-1}$  at 50 mA g $^{-1}$ ) and stable cycling performance (92.1% capacity retention after 100 cycles at 100 mA g $^{-1}$ ) was achieved for the tin asymmetric membrane electrode synthesized using polysulfone and tin tert-butoxide precursor

# Data availability

The raw/processed data required to reproduce these findings cannot be shared at this time due to legal or ethical reasons.

# CRediT authorship contribution statement

Mengya Li: Investigation, Writing - original draft. Christopher Anderson: Methodology, Investigation. Parker Beaupre: Methodology, Investigation. Congrui Jin: Investigation, Resources. Jianlin Li: Conceptualization, Supervision. Ji Wu: Conceptualization, Methodology, Resources, Investigation, Supervision, Project administration, Funding acquisition.

# **Declaration of Competing Interest**

The authors declare that they have no known competing financial interests or personal relationships that could have appeared to influence the work reported in this paper.

# Acknowledgement

This study is supported by National Science Foundation Division of

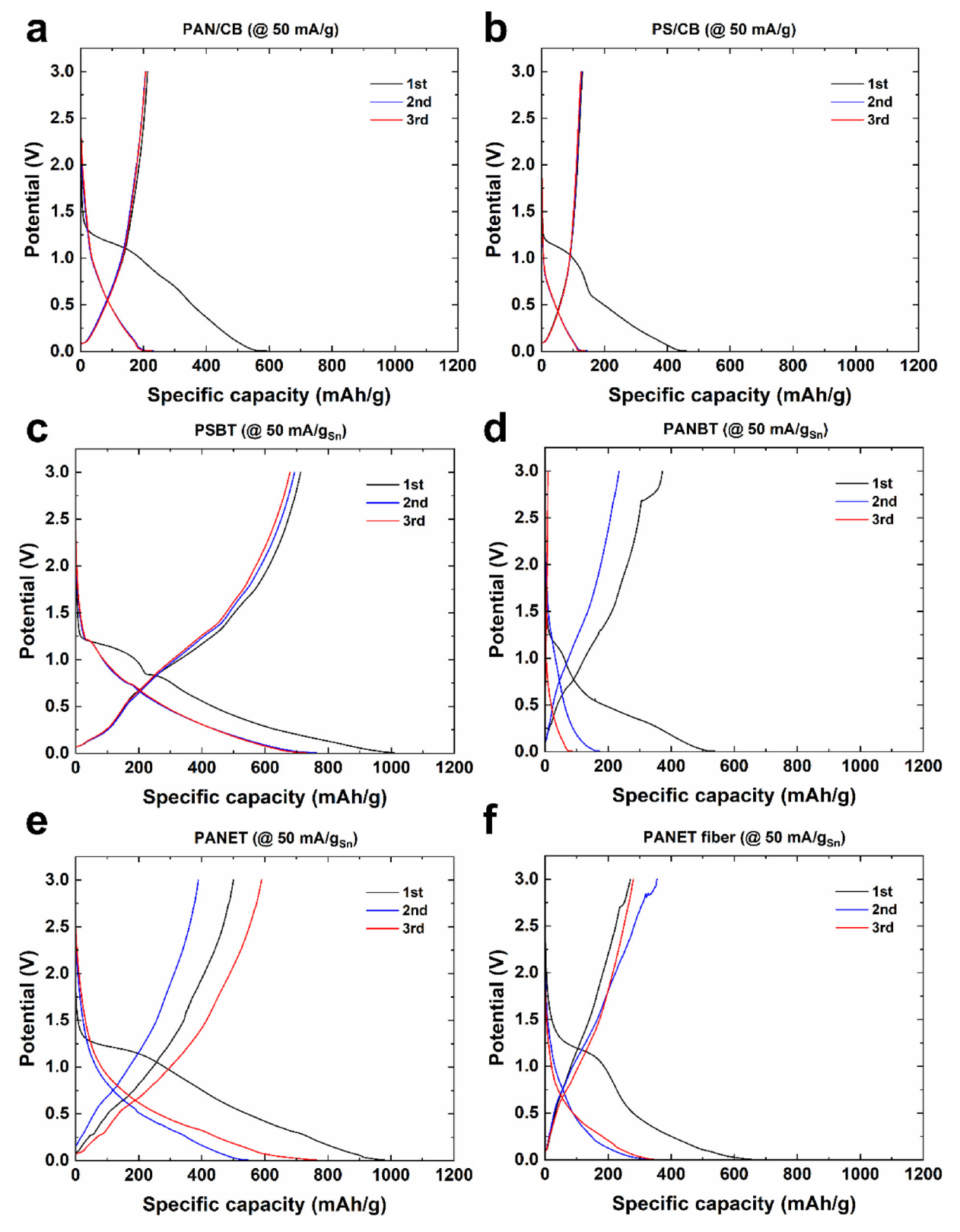


Fig. 5. Galvanostatic charge/discharge curves of the first three cycles of a) PAN/CB, b) PS/CB, c) PSBT, d) PANBT, e) PANET, and f) PANET fiber within 0.01 - 3 V at a current density of  $50 \text{ mA g}^{-1}$ .

Chemical, Bioengineering, Environmental and Transport Systems NSF CBET Award #1800619. JW, CA, PB and CJ deeply appreciate the infrastructural support from Georgia Southern University and Binghamton University. This work also made use of the Cornell Center for Materials Research Shared Facilities which are supported through

the NSF MRSEC program (DMR-1719875). The homebuilt setup for the fiber extrusion was kindly fabricated by Prof. Shaowen Xue at the Mechanical Engineering Department of Georgia Southern University.

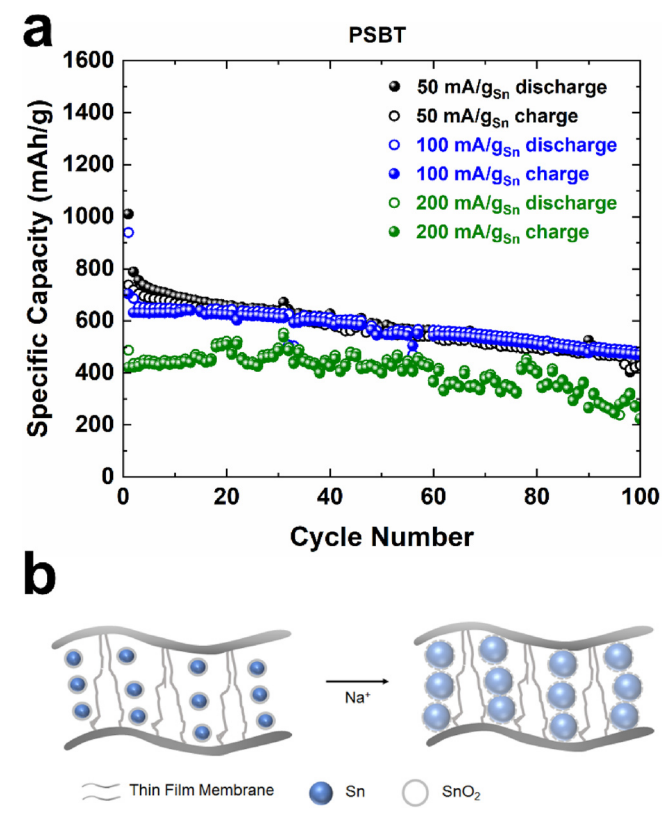


Fig. 6. a) Cycling performance of PSBT at 50, 100, and 200 mA  $g_{Sn}^{-1}$  rates; b) schematic illustration of the sodiation process for PSBT asymmetric membrane.

# Appendix A. Supplementary data

Supplementary material related to this article can be found, in the at doi:https://doi.org/10.1016/j.mtcomm.2020. online 100998.

# References

[1] M.R. Palacín, Chem. Soc. Rev. 38 (9) (2009) 2565.

- [2] K. Kang, et al., Science 311 (5763) (2006) 977.
- [3] M. Armand, J.M. Tarascon, Nature 451 (2008) 652.
- [4] L. Gaines, Sustain. Mater. Technol. 1-2 (2014) 2.
- [5] L. Li, et al., Energy Environ. Sci. 11 (9) (2018) 2310.
- [6] M.D. Slater, et al., Adv. Funct. Mater. 23 (8) (2013) 947.
- [7] S.-W. Kim, et al., Adv. Energy Mater. 2 (7) (2012) 710.
- [8] C. Vaalma, et al., Nat. Rev. Mater. 3 (4) (2018) 18013.
- [9] M.H. Han, et al., Energy Environ. Sci. 8 (1) (2015) 81.
- [10] N. Yabuuchi, et al., Chem. Rev. 114 (23) (2014) 11636.
- [11] Z. Shadike, et al., Adv. Energy Mater. 8 (17) (2018) 1702588.
- [12] M. Lao, et al., Adv. Mater. 29 (48) (2017) 1700622. [13] J.W. Wang, et al., Nano Lett. 12 (11) (2012) 5897.
- [14] D.-H. Nam, et al., ACS Nano 8 (11) (2014) 11824.
- [15] Y. Liu, et al., Adv. Mater. 27 (42) (2015) 6702.
- [16] H. Zhu, et al., Nano Lett. 13 (7) (2013) 3093.
- [17] Y. Yu, et al., Adv. Mater. 19 (7) (2007) 993.
- [18] J. Qin, et al., ACS Nano 8 (2) (2014) 1728.
- [19] C. Xu, et al., ACS Appl. Mater. Interfaces 5 (24) (2013) 12911.
- [20] Y. Wang, et al., J. Power Sour. 219 (2012) 89.
- [21] T. Palaniselvam, et al., Adv. Funct. Mater. 29 (18) (2019) 1900790.
- [22] N. Zhang, et al., Chem. Commun. 54 (10) (2018) 1205.
- [23] D. Su, et al., Chem. Commun. 49 (30) (2013) 3131.
- [24] Y.C. Lu, et al., J. Power Sour. 284 (2015) 287.
- [25] H. Ying, W.-Q. Han, Adv. Sci. 4 (11) (2017) 1700298.
- [26] J.-Y. Hwang, et al., Chem. Soc. Rev. 46 (12) (2017) 3529.
- [27] K.P. Lee, et al., J. Membr. Sci. 370 (1) (2011) 1.
- [28] I. Byrd, J. Wu, Electrochim. Acta 213 (2016) 46.
- [29] M. Ulbricht, Polymer 47 (7) (2006) 2217.
- [30] I. Pinnau, W.J. Koros, J. Membr. Sci. 43 (8) (1991) 1491.
- [31] I.-C. Kim, et al., J. Membr. Sci. 199 (1) (2002) 75.
- [32] Z. Fan, et al., J. Membr. Sci. 320 (1) (2008) 363.
- [33] H.-S. Min, et al., J. Power Sour. 119-121 (2003) 469.
- S. Nejati, et al., J. Membr. Sci. 492 (2015) 355. [34]
- [35] E. Zussman, et al., Carbon 43 (10) (2005) 2175.
- [36] C. Kim, et al., J. Raman Spectrosc. 35 (11) (2004) 928. [37] J. Wu, et al., Energy Technol. 4 (4) (2016) 502.
- C. Fritzmann, et al., Desalination 216 (1) (2007) 1. [38]
- [39] A.C. Ferrari, Solid State Commun. 143 (1) (2007) 47.
- [40] C. Meier, et al., Physica E: Low. Syst. Nanostruct. 32 (1) (2006) 155.
- [41] B. Eifert, et al., Phys. Rev. Mater. 1 (1) (2017) 014602.
- [42] K. Nogita, et al., Philos. Mag. 93 (27) (2013) 3627. [43] Z. Li, et al., Acc. Chem. Res. 48 (6) (2015) 1657.
- [44] M. Wu, et al., Ionics 19 (10) (2013) 1341.
- [45] L. Alexander, H.P. Klug, J. Appl. Phys. 21 (2) (1950) 137.
  [46] O.A. Chuvenkova, et al., Phys. Solid State 57 (1) (2015) 153.
- [47] R.O. Ansell, et al., J. Electrochem. Soc. 124 (9) (1977) 1360.
- [48] H.L. Zhu, et al., Nano Lett. 13 (7) (2013) 3093.
- [49] Y.H. Xu, et al., Adv. Energy Mater. 3 (1) (2013) 128.
- [50] Y.H. Liu, et al., ACS Nano 7 (4) (2013) 3627.
- [51] M.K. Datta, et al., J. Power Sour. 225 (2013) 316.